Charge localization and magnetocrystalline anisotropy in La, Pr, and Nd substituted Sr hexaferrites

Vojtěch Chlan,* Karel Kouřil, Kateřina Uličná, and Helena Štěpánková
Faculty of Mathematics and Physics, Charles University in Prague, V Holešovičkách 2, 18000 Prague 8, Czech Republic

Jörg Töpfer and Daniela Seifert
University of Applied Sciences Jena, Dept. SciTec, Carl-Zeiss-Promenade 2, 07745 Jena, Germany
(Received 27 February 2015; published 14 September 2015)

Charge compensation in strontium M-type hexaferrites $A_x^{3+}Sr_{1-x}Fe_{12}O_{19}$ (A = La, Nd, or Pr) is studied by means of calculations of electronic structure and ^{57}Fe nuclear magnetic resonance (NMR) experiments. Two different states are realized in the calculations: a localized scenario as a ground state with the extra valence charge preferentially in the octahedral 2a sites and a delocalized scenario with the charge delocalized over multiple sites. From the calculations and NMR experiments, it is deduced that the localized state Fe^{2+}(2a) occurs at low temperatures regardless of the type of used substitution and that the distribution of ferric and ferrous ions within the 2a sublattice is static at low temperatures. The magnetocrystalline anisotropy energy of Sr and La hexaferrites is calculated and the contributions of individual Fe sublattices are evaluated. The temperature dependence of the anisotropy for La hexaferrite is explained as a transition between localized and delocalized states causing changes in the single ion contributions of Fe in 2a and also 12k sites.

DOI: 10.1103/PhysRevB.92.125125 PACS number(s): 32.10.−f, 76.60.−k, 75.30.Gw

I. INTRODUCTION

Hexagonal ferrites [1–3] are well established ferrimagnetic materials with many uses: they can be found in cost-effective hard magnets as well as in components for high-frequency applications. Interest in hexaferrites has been rekindled by the discovery of intrinsic magnetoelectrics with strong coupling of magnetic and electric order as well as by the emergence of various low-dimensional hexaferrite systems, e.g., nanoparticles, fibres, thin layers, or composites [4]. Finally, there is still effort devoted to classical hexaferrite systems aimed on improving their performance in applications and unveiling related physics.

One of the important properties of strontium M-type hexaferrite $SrFe_{12}O_{19}$ (SrM) is the magnetocrystalline anisotropy. The anisotropy arises mainly from contributions of ferric cations. In the hexaferrite structure (space group $P6_3/mmc$), Fe atoms occupy sites 2a, 2b, $4f_{IV}$, $4f_{VI}$, and 12k, which form five magnetic sublattices (see Fig. 1). The magnetocrystalline anisotropy of SrM is uniaxial with the easy axis of magnetization parallel to the hexagonal axis, but the way how the individual Fe sublattices add up to the total anisotropy is less clear, as the contributions of individual sublattices are difficult to obtain experimentally. These contributions have thus been estimated indirectly, e.g., from changes of the measured anisotropy in substituted hexaferrites [5–7], or calculated as single-ion contributions using appropriate spin Hamiltonians and considering the symmetry of the crystal field [8–10]. It became generally accepted that mainly Fe^{3+} in 2b sites are responsible for the uniaxial character of anisotropy in Sr (and Ba) M-type hexaferrites [11] and that the contributions of other ferric cations, especially the 12k, are also important [8–10].

The magnetocrystalline anisotropy due to ferric ions can be altered by replacing the Fe with suitable substitutions [12–15] as well as by substituting the Sr by a trivalent cation [16–18]. Particularly, in La^{3+} M-type hexaferrites (LaM), the observed magnetocrystalline anisotropy increases with decreasing temperature, in contrast to almost a constant character of the temperature dependence for Sr or Ba M-type hexaferrites [19,20]. At low temperatures, the anisotropy of La hexaferrites was found two times higher than the value for Sr or Ba hexaferrites. Based on measurements of the anisotropy field and total magnetic moment, it was proposed by Lotgering [19] that the increased anisotropy at low temperatures is due to the formation of Fe^{2+} in octahedral 2a sites.

Although the Fe^{2+}(2a) localization was supported by local hyperfine methods [16,20–24], the mechanism of increased magnetic anisotropy proposed by Lotgering is still an open question. In published calculations of the electronic structure of these hexaferrites [25,26], the localized state was not reached—the calculations resulted in a delocalized solution with excess charge contained in the interstitial space or smeared over all iron sites, which is not in accord with the conclusions of the experiments. Since the explanation of how the charge compensation and anisotropy are connected is lacking, this issue is addressed in the present paper.

The aim of this work is to understand the increase of magnetocrystalline anisotropy in La hexaferrite at low temperatures, and to explain the relation of this increase to the presence of Fe^{2+}. For this purpose, we studied M-type hexaferrites $A_x^{3+}Sr_{1-x}Fe_{12}O_{19}$ (A = La, Nd, or Pr) by means of electronic structure calculations and nuclear magnetic resonance experiments. Contrary to previous calculations [25,26], we found the ground state with Fe^{2+} in 2a sites for all studied systems with A^{3+}. Such localization was also confirmed by our NMR experiments. Based on calculations, we present a mechanism of increased (decreased) magnetocrystalline anisotropy in La hexaferrites at low (high) temperatures.

II. METHODS

A. Electronic structure calculations

Our calculations used the augmented plane waves + local orbital method based on the density functional theory (DFT)

*vojtech.chlan@mff.cuni.cz

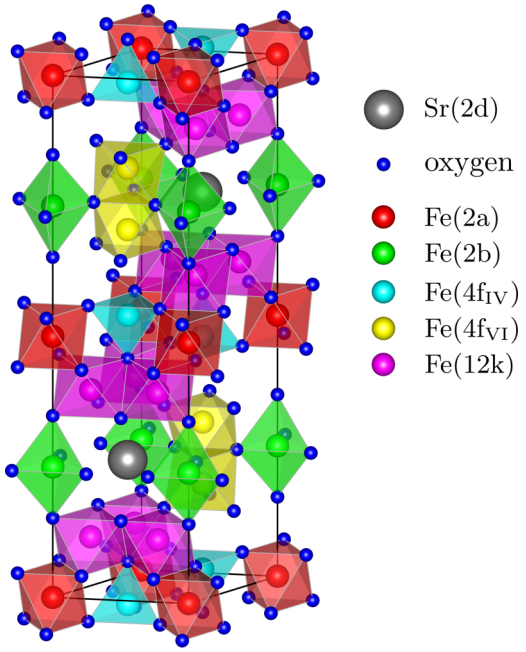

FIG. 1. (Color online) Unit cell of hexaferrite $SrFe_{12}O_{19}$. The five nonequivalent Fe sites are octahedral 2a (site symmetry $\bar{3}m$), bipyramidal 2b ($\bar{6}m2$), tetrahedral $4f_{IV}$, octahedral $4f_{VI}$ (both $3m$), and 12k (site symmetry m). The three- and sixfold local axes are parallel to the hexagonal axis c of the crystal (vertical direction in the picture), which is also the easy axis of magnetization.

as implemented in WIEN2K [27]. For the exchange-correlation functional, the PBE-GGA form was adopted [28]. To improve the description of iron $3d$ electron correlations, we used the rotationally invariant version of the LDA+U method [29] with the GGA instead of LSDA exchange-correlation potential and with a single parameter $U_{\text{eff}} = U - J$.

The electronic structure of hexaferrites, with unit cells containing two formula units $AFe_{12}O_{19}$ (A = Sr, La, Nd, and Pr), were calculated within space group $P6_3/mmc$; the lattice constants that were used are displayed in Table I. There are eleven nonequivalent atomic sites in the structure including the five Fe sites. The magnetic structure was considered as collinear, with the moments of Fe atoms in 2a, 2b, and 12k sites being antiparallel to the moments of Fe in $4f_{IV}$ and $4f_{VI}$ sites.

The calculation of the electronic structure of mixed LaSr hexaferrite $La_{0.5}Sr_{0.5}Fe_{12}O_{19}$ was performed within space group $P\bar{6}m2$, where the number of nonequivalent atoms increased to 21, as only the 2a octahedra retained their multiplicity 2; all other sites split 1:1. As a comparison, calculations were performed for a low-temperature structure of $LaFe_{12}O_{19}$ with the orthorhombic $Cmcm$ space group proposed by Küpferling *et al.* [24]. This structure loses hexagonal symmetry due to orthorhombic distortion: the 12k site of the original hexagonal structure splits into 16h and $8f_3$, otherwise there is one-to-one correspondence between hexagonal (2a, 2b, $4f_{IV}$, $4f_{VI}$) and orthorhombic sites (4a, 4b, $8f_1$, $8f_2$).

TABLE I. Lattice parameters in angstroms used by the presented calculations.

Structure	a	b	c
SrM	5.9618	5.9618	23.3533
LaSrM	5.9373	5.9373	23.1962
LaM, PrM, NdM	5.9128	5.9128	23.0391
LaM (orthorhombic) [24]	5.9025	10.1593	22.7883

The atomic positions of all calculated structures were optimized within their space groups by minimization of the total energy and atomic forces. The lattice parameters (Table I) of Sr and La hexaferrites were optimized with $RK_{max} = 7.0$. The lattice parameters of La hexaferrite were then used also for Nd and Pr hexaferrites (NdM, PrM), while those of the mixed LaSr hexaferrite (LaSrM) were interpolated from Sr and La structures. The lattice parameters of the orthorhombic structure were not optimized, we used the parameters acquired by Küpferling *et al.* [24].

The radii of the atomic spheres were chosen as 1.45 a.u. for oxygen, 2.0 a.u. for iron, and 2.5 a.u. for large cations (La, Sr, Nd, or Pr). The dependence on the size of the basis, the number of k points, and the high-energy cutoff was tested on the Sr hexaferrite where the energy of magnetocrystalline anisotropy was satisfactorily converged already for $RK_{max} = 6.0$ (APW+lo method), k-mesh $7 \times 7 \times 1$, and $E_{max} = 5.0$ Ry. The charge density was Fourier expanded to $G_{max} = 16\sqrt{\text{Ry}}$ and the value of parameter $U_{\text{eff}} = 4.5$ eV was adopted for the $3d$ orbitals of iron atoms; its influence on the calculated quantities is discussed in the text.

The self-consistent calculation of the magnetocrystalline anisotropy is a difficult task as the corresponding energy differences of the order of 1–10 μRy/atom are comparable to the energetic resolution of available full potential calculations. The results obtained in a self-consistent calculation are thus overly sensitive to various calculational parameters (size of the basis set, number of k points). Since in case of these hexaferrites the spin-orbit coupling is small compared to $3d$ bandwidth or the exchange splitting, the anisotropies of the studied compounds can be studied using the force theorem approach, where the spin-orbit coupling is introduced non-self-consistently (for details and further references see Ref. [30]). Our practice was as follows: the spin-polarized calculation was converged self-consistently without spin-orbit coupling, using such a set of symmetry operations that satisfied all intended [hkl] directions of magnetization. Then, starting from the converged potential, the eigenvalue problem was solved for each direction with the spin-orbit coupling switched on non-self-consistently, i.e., within one iteration only. The difference in total energies was then evaluated for different [hkl] directions to determine the magnetocrystalline anisotropy. This spin-orbit interaction was applied within the atomic spheres using the second variational method, which allowed us to resolve the contributions of individual Fe sublattices to anisotropy.

B. Hexaferrite samples

The studied powder samples of hexaferrites with a substitution of the large cation were prepared by the standard ceramic process (for details see Refs. [16,31]). In the case of the $La_xSr_{1-x}Fe_{12}O_{19}$ system, the samples covered the whole

concentration range—five samples with $x = 0$, 0.25, 0.5, 0.75, and 1. For Nd and Pr substitutions, the single phase limits are 0.375 for Pr and below 0.37 for Nd; we studied the samples $Nd_xSr_{1-x}Fe_{12}O_{19}$ ($x = 0.125$, 0.250, and 0.300) and $Pr_xSr_{1-x}Fe_{12}O_{19}$ ($x = 0.125$, 0.250, and 0.375). The single-phase samples were characterized by powder XRD, microscopy, electron-probe microanalysis, thermal analysis, magnetic measurements, and Mössbauer spectroscopy [31].

C. ^{57}Fe nuclear magnetic resonance experiments

Frequency-swept ^{57}Fe NMR spectra were recorded in zero external field at 4.2 K using spectrometer console Bruker Avance and a home-made probe. The nuclear spin of ^{57}Fe is $\frac{1}{2}$ and the magnetogyric ratio $\gamma = 1.38$ MHz T^{-1}, so that the resonance frequency corresponds directly to the local magnetic field. A tuned and well matched resonance circuit in the probe was used and special care was given to ensure reliable intensities of NMR spectra in the whole frequency range. The Carr-Purcell-Meiboom-Gill (CPMG) pulse sequence was applied and the pulse lengths and amplitudes were set to excite the signal of nuclei in the magnetic domains. Depending on the sample composition, the required lengths of $\frac{\pi}{2}$ pulses were 1.5–10 μs, the frequency step in spectra 10–50 kHz, and the delay between scans 1–150 s. Spin echoes formed within the CPMG sequence were detected and coherently summed in the time domain. The signals obtained at individual excitation frequencies were then Fourier transformed to the frequency domain. To minimize the modulation of spectra by T_2 relaxation, only the first five recorded echoes were used for evaluation. The final spectrum was constructed as an envelope of the particular FT lines and a frequency correction $1/f^3$ of spectral intensity was applied.

III. RESULTS AND DISCUSSION

In the first part of this section, we describe how the state with Fe^{2+} localized in 2a was reached in DFT calculations. Then the results of calculations and experiments regarding the localization are presented. The last part concerns magnetocrystalline anisotropy: its calculation, comparison with available experimental data, and also discussion of the results.

A. Charge localization from DFT calculations

The GGA+U method improves the description of iron 3d electron correlations and in the case of hexaferrites provides correctly the insulating ground state, while with GGA, the ground state would be almost metallic [25]. However, one has to be careful when using the GGA+U method on complex structures as there is a danger that an incorrect electron density is stabilized by the applied orbital potential. The calculation then becomes trapped in some local energy minimum, which may depend on the starting conditions, the process of including the orbital potential, or various parameters of the calculation (e.g., mixing scheme). On the other hand, the fact that GGA+U stabilizes (and amplifies) inequivalency and leads to a charge disproportionation can be exploited in order to search for energetic minima that a pure GGA calculation would not reach. When more than one stable self-consistent solutions are obtained, apparently, it is justified to choose the one with the lowest total energy as the correct solution. Our approach to obtain and evaluate such energy minima is thus similar to the common practice for the calculation of magnetic exchange interactions from the differences of the total energies of states with different atomic spin configurations [32–35]. Instead of starting the self-consistent calculations with various orientations of atomic spins, our procedure is more subtle: calculations start with the same spin structure but we modify the initial occupations of electronic states.

Local energy minima for La M-type hexaferrite (LaM) $LaFe_{12}O_{19}$ were searched by arranging several different occupations of valence electrons of Fe atoms in the initial electron density. The calculation for each of these density templates was then carried out without any further interventions in the population matrices until it self-consistently converged using GGA+U with $U_{\text{eff}} = 4.5$ eV. All calculations reached either a solution corresponding to a delocalized scenario with all iron atoms being Fe^{3+}-like, or a solution having Fe^{2+} localized in the 2a site, as was indicated by the lowered magnetic moment of Fe(2a) in Table II. The latter, localized solution had the total energy lower by ≈0.64 eV and thus was declared as the ground state. Between two calculations with different starting conditions but reaching the same type of solution only slight variations of calculated quantities were observed (≈0.001 μ_B in atomic moments and below 0.1 meV in total energy). Such differences were not attributed to additional solutions since they are close to the precision threshold of our DFT calculations, which was estimated as ≈0.01 meV.

Analogous calculations were carried out for pure Sr, Nd, and Pr hexaferrites, the mixed La/Sr hexaferrite, and also for the La hexaferrite with the orthorhombic structure proposed by Küpferling *et al.* [24]. For structures with a trivalent large atom, we again found a delocalized and a localized solution, the latter being energetically favorable. As expected, for Sr hexaferrites, such calculations found only a single solution with all Fe ions in a ferric state (Table II). Similarly to the situation in La hexaferrites, for all structures with a trivalent large cation, the localized solution was assigned to the ground

TABLE II. Magnetic moments (in μ_B units) and valences of atoms in La and Sr M-type hexaferrites. The moments were calculated inside generalized atomic volumes using the atoms-in-molecules (AIM) method. The valence was obtained as the difference of the integrated electronic charge inside the AIM volume and the atomic number Z.

	magnetic moment (μ_B)			valence		
atom	SrM	LaM deloc.	LaM loc.	SrM	LaM deloc.	LaM loc.
Fe(2a)	4.20	4.12	3.63	1.84	1.76	1.42
Fe(2b)	4.11	4.11	4.11	1.77	1.76	1.76
Fe($4f_{IV}$)	−4.11	−4.11	−4.10	1.79	1.78	1.77
Fe($4f_{VI}$)	−4.15	−4.17	−4.17	1.86	1.85	1.85
Fe(12k)	4.20	4.16	4.22	1.82	1.77	1.82
O(4e)	0.42	0.40	0.42	−1.23	−1.24	−1.23
O(4f)	0.10	0.08	0.14	−1.24	−1.25	−1.25
O(6h)	0.03	0.04	0.04	−1.24	−1.23	−1.22
O($12k_1$)	0.10	0.08	0.06	−1.24	−1.25	−1.25
O($12k_2$)	0.21	0.14	0.15	−1.22	−1.23	−1.23
La/Sr(2d)	0.00	−0.02	0.00	1.65	2.15	2.15

TABLE III. The formal valence states for all studied hexaferrite structures. The values were obtained by normalizing the valences (extracted from AIM method) by a factor ≈0.62, which scaled the average charge of oxygen atoms to the value of −2, representing the oxidation state O^{2-}. Label of cation A stands for Sr, La, Nd, or Pr.

		LaM		PrM		NdM		LaSrM		
atom	SrM	deloc.	loc.	deloc.	loc.	deloc.	loc.	atom	deloc.	loc.
Fe(2a)	2.99	2.84	2.30	2.87	2.35	2.91	2.58	Fe(2a)	2.92	2.70
Fe(2b)	2.87	2.84	2.85	2.84	2.86	2.84	2.86	Fe(2b′)	2.84	2.85
								Fe(2b″)	2.86	2.86
$Fe(4f_{IV})$	2.89	2.87	2.86	2.88	2.86	2.88	2.87	$Fe(4f'_{IV})$	2.88	2.88
								$Fe(4f''_{IV})$	2.89	2.88
$Fe(4f_{VI})$	3.01	2.98	2.99	2.99	2.99	2.99	2.99	$Fe(4f'_{VI})$	2.99	2.99
								$Fe(4f''_{VI})$	2.99	3.00
Fe(12k)	2.95	2.86	2.95	2.88	2.95	2.90	2.94	Fe(12k′)	2.94	2.94
								Fe(12k″)	2.87	2.93
A(2d)	2.67	3.47	3.49	3.28	3.38	3.13	3.21	Sr(2d)	2.67	2.67
								La(2d)	3.49	3.50

state, while the delocalized solution was found approximately 0.5 eV higher in energy.

The valence states of Fe cations in hexaferrites can be estimated from their calculated magnetic moments, since all Fe cations are expected to be in high spin states, i.e., free iron ion possessing a magnetic moment of 5 μ_B or 4 μ_B is nominally Fe^{3+} or Fe^{2+}, respectively. In a crystal, the calculated moments are lower, because of the hybridization effect of iron 3*d* orbitals with oxygen orbitals, which is a physically correct picture. However, a fraction of the magnetic moment leaks out of the atomic spheres, and thus is not attributed to any specific atom. We avoid this undesired effect by using the AIM approach [36], where for the purpose of evaluating the atomic valences or magnetic moments, generalized atomic volumes are calculated and used instead of the original atomic spheres. The valences from the AIM analysis are presented in Table III. For easier differentiation between Fe^{2+} and Fe^{3+} states we introduce formal valence states obtained by normalizing the calculated atomic charges by such a factor (≈0.62) that would bring the average charge of oxygen ions to the value of −2, representing the oxidation state O^{2-}. These formal valence states for Fe atoms in all calculated hexaferrites are displayed in Tables III and IV.

From a survey of Table III, one finds the Fe cations in the Sr hexaferrite on average to possess a formal valence state 2.95, i.e., essentially Fe^{3+} states. As expected due to the presence of an extra valence charge, the averaged formal valence state of Fe in the La hexaferrite (2.88) is somewhat lower than in the Sr hexaferrite and is practically the same for both localized and delocalized solutions of the La hexaferrite. Roughly, half of the extra charge is localized at lanthanum for both types of solutions. In the case of the delocalized solution, the remaining charge is distributed among Fe cations (especially in 2a and 12k sites) and oxygens. For the localized solution, however, the excess charge is almost exclusively at the 2a sites, as indicated by its reduced valence state. This behavior can be observed also in data for NdM and PrM (Table III) and analogous charge compensation is found also in the orthorhombic LaM structure (Table IV). Furthermore, the localization, albeit a weak one, can be observed also in the mixed $(LaSr)_{0.5}Fe_{12}O_{19}$ (LaSrM) hexaferrite (Table III). All these results indicate that the Fe^{2+} appears in the octahedral 2a sites regardless of the choice of the trivalent large cation (La, Nd, or Pr). Moreover, this localization effect is not inherent to the hexagonal structure: Fe^{2+} is present (in 4a sites) also in the orthorhombic structure.

Besides the abrupt change of valence of Fe in 2a sites (respectively, 4a in the orthorhombic structure) for all localized solutions, we can notice differences also in delocalized solutions. Compared to SrM, the valence states of Fe cations in 2a and 12k sites of LaM are lower, while the other Fe cations remain relatively intact. In the mixed structure LaSrM, where the 12k sublattice splits into two, only the six Fe(12k″) cations, which are near the La^{3+} sites display such a difference. In the delocalized state, the extra minority charge thus slightly prefers the 2a sites and those 12k sites that are close to the trivalent large cation.

TABLE IV. The formal valence states extracted from AIM method are displayed for the orthorhombic structure of La hexaferrite proposed by Küpferling *et al.* [24]. The values were obtained by normalizing the valences (extracted from AIM method) by a factor ≈0.62, which scaled the average charge of oxygen atoms to the value of −2, representing the oxidation state O^{2-}.

atom	deloc.	loc.
Fe(4a)	2.72	2.39
Fe(4b)	2.81	2.84
$Fe(8f_1)$	2.94	2.94
$Fe(8f_2)$	2.97	2.97
$Fe(8f_3)$	2.83	2.88
Fe(16h)	2.89	2.94
La(4c)	3.44	3.46

B. Charge localization from ^{57}Fe NMR experiments

Zero field ^{57}Fe NMR spectra of the Sr hexaferrite, La, Nd, and Pr substituted Sr hexaferrites, and the La hexaferrite measured at 4.2 K are displayed in Fig. 2. The Sr hexaferrite spectrum contains five lines corresponding to five sublattices 2b, 12k, $4f_{IV}$, 2a, and $4f_{VI}$ (listed by increasing frequency). With increasing concentration of La, Nd, or Pr, the local environment of ^{57}Fe nuclei is perturbed: the local symmetry

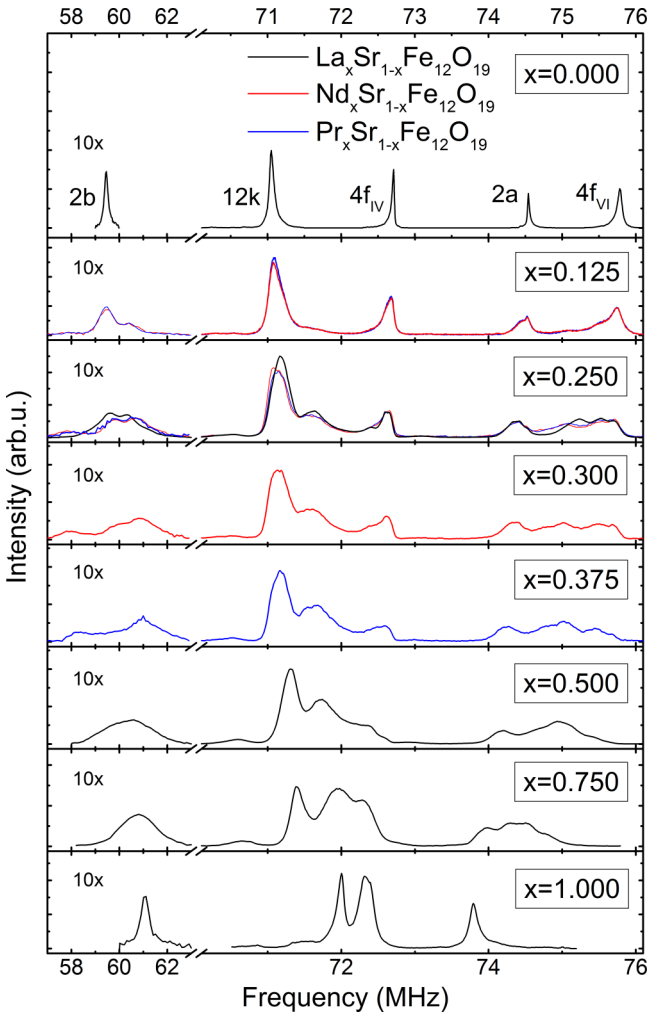

FIG. 2. (Color online) ^{57}Fe NMR spectra of the Sr hexaferrite ($x = 0$), La, Nd, and Pr substituted Sr hexaferrites ($x \in \langle 0.125, 0.75 \rangle$), and the La hexaferrite ($x = 1$) measured at 4.2 K in zero external field. Spectra are sorted with increasing concentration x of the trivalent large cation from top to bottom; the weak resonance of 2b at lower frequencies is scaled 10x.

of Fe sites is reduced by the substituent, which causes visible line splitting for the neighboring Fe sites or line broadening when the sites are further away. Additionally, these changes manifest also as gradual shifts in resonance frequency; see the shift of center of mass of 2b line in Fig. 3.

The spectra in the frequency range of 71–76 MHz noticeably follow a common trend regardless of the type of substituting atom. On the other hand, the Fe(2b) subspectrum at lower frequencies differs for Nd and Pr substituted samples from that of La substituted hexaferrite. This is attributed to the fact that Nd and Pr both possess a magnetic moment. Since 2b are the nearest iron sites to the large cation site (see Fig. 1), the Fe(2b) resonance is visibly affected by an additional field due to the interaction with the magnetic moment of Nd or Pr. Analogous yet smaller differences can be observed in Fig. 2 (panel $x = 0.25$) for 12k and 4f$_{VI}$ spectral lines, as the 12k and 4f$_{VI}$ sites are the next nearest neighbors to the large cation site. And finally, the effect on 4f$_{IV}$ and 2a lines is negligible as these sites are the most distant to the large cation in 2d site.

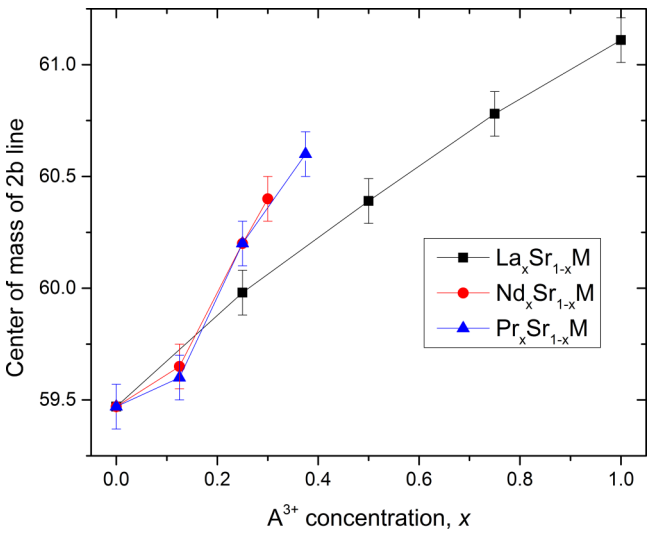

FIG. 3. (Color online) Shift of 2b line resonance frequency (evaluated as a center of mass) in dependence on the concentration of trivalent large cation. Lines are only a guide for the eye.

The resonance line of ^{57}Fe in 2a sites is interesting, its intensity diminishes with increasing concentration of La, Nd, or Pr, while the resonance frequency remains rather constant. The loss of 2a line intensity is attributed to the change of the valence state of some of the Fe(2a) ions towards Fe^{2+} state. Such a change is accompanied by a decrease of Fe 3d magnetic moment, which in turn decreases the local hyperfine magnetic field, i.e., the resonance frequency of ^{57}Fe in Fe^{2+}(2a) is significantly shifted to lower frequencies with respect to the position of ^{57}Fe in Fe^{3+}(2a). This is in accord with the results of Mössbauer spectroscopy by Seifert *et al.* [31] who found the hyperfine field of ^{57}Fe in Fe^{2+}(2a) approximately 10 T lower than the field of ^{57}Fe in Fe^{3+}(2a) in Sr hexaferrites partially substituted by La, Nd, Pr, or Sm at room temperature. At lower temperatures, this difference increases to more than 20 T as was observed by Grössinger *et al.* in a La hexaferrite [20].

Direct measurement of Fe^{2+} by ^{57}Fe NMR is difficult, probably due to the rapid spin-spin relaxations and line broadening; the formation of Fe^{2+}(2a) is thus observed indirectly as a decrease of the Fe^{3+}(2a) intensity. Due to the overlap of some of the spectral lines, the intensities were evaluated for groups: (12k + 4f$_{IV}$) and (2a + 4f$_{VI}$). The intensity of (2a + 4f$_{VI}$) lines decreases linearly with increasing concentration of the trivalent large ion while the intensity of (12k + 4f$_{IV}$) remains constant for all concentrations (Fig. 4).

Because of the La-Sr disorder, the 4f$_{VI}$ line is split into four overlapping components with unknown asymmetric profiles, therefore, a quantitatively reliable decomposition of the (2a + 4f$_{VI}$) profile into contributions of the 2a and 4f$_{VI}$ sublattices is not possible. From a qualitative comparison of spectral profiles, it is evident that the observed decrease of the (2a + 4f$_{VI}$) intensity is due to the decrease of the 2a line intensity. From the dependence of NMR line intensities, we thus confirm that at low temperatures, the Fe^{2+} cations form in 2a sites to compensate the addition of trivalent substitution.

Apparently, the character of the changes is uniform regardless of the type of used substitution, which is in a very

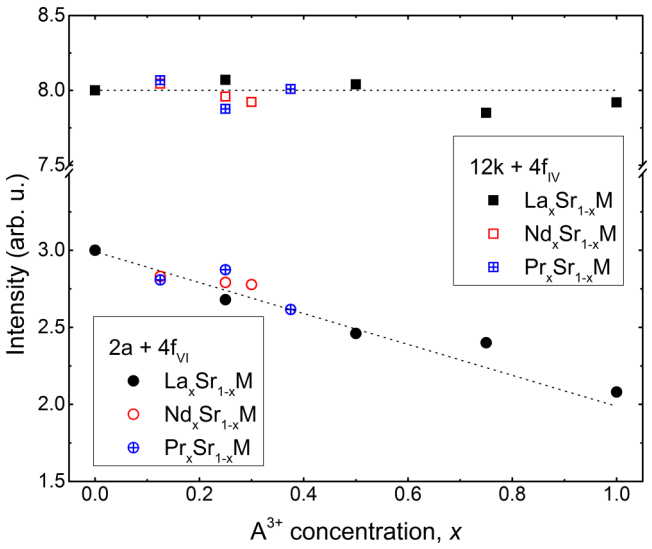

FIG. 4. (Color online) Integral intensities of $12k + 4f_{IV}$ and $2a + 4f_{VI}$ resonance lines depending on the concentration of the trivalent large cation. Lines correspond to nominal numbers of Fe^{3+} atoms per formula unit $A_x^{3+}Sr_{1-x}Fe_{12}O_{19}$ for the scenario with the Fe^{2+} cation occupying the 2a sites, i.e., eight atoms for $12k + 4f_{IV}$ and $3 - x$ atoms for $2a + 4f_{VI}$. The total integral intensities of the four considered spectral lines were normalized to $11 - x$.

good agreement with our calculations for structures with a trivalent A^{3+} large cation. The calculated La, Nd, and Pr hexaferrites exhibit a ground state with localized Fe^{2+}, while the other Fe ions remain ferric. The NMR and DFT results are also consistent in finding that the number of ferric ions in the 2a sublattice changes gradually with concentration x. Although only one structure with a mixed content of La and Sr is available from calculations (see Table III), the formal valence state of its Fe(2a) is between the values of Fe^{3+}(2a) in SrM and Fe^{2+}(2a) in LaM.

The linear decrease of Fe^{3+}(2a) intensity in our NMR spectra also indicates that the distribution of Fe^{2+} in the 2a sublattice is rather static at low temperatures. Significant fast electron hopping within the 2a sublattice would induce a gradual decrease of resonance frequency with increasing concentration of substitution because of the decrease of the local field—the observed field would have been the weighted average of Fe^{2+} and Fe^{3+} fields. Such a rapid shift of the 2a line frequency with increasing concentration of substitution is not observed in our NMR spectra. Furthermore, the NMR relaxation times would be shortened due to the increasingly ferrous character of ions, which is again not the case as the relaxation times of the 2a line do not significantly differ from the values of other resonance lines. Therefore we can conclude that there are well defined ferric and ferrous ions in the 2a sublattice and their arrangement at low temperatures does not change significantly on the time scale of at least 100 μs (typical duration of performed NMR experiments at $T = 4.2$ K). While these findings are in agreement with the Mössbauer measurements of Seifert *et al.* [31] performed on the same set of samples, they are in contrast with the ^{57}Fe NMR results by Küpferling *et al.* [24] who reported no loss of 2a intensity (up to $x_{La} = 0.3$).

C. Calculation of magnetocrystalline anisotropy

The magnetocrystalline anisotropy of La and Sr hexaferrites was calculated within the force theorem approach as described in Sec. II. The energy of magnetocrystalline anisotropy was evaluated as $E_{MA} = E_{\perp} - E_{||}$, where $E_{||}$ stands for the total energy with the direction of the magnetization in the hexagonal axis, while $E_{\perp}$ denotes the averaged energy of calculations with the magnetization in the hexagonal plane. In our calculations, the variations of such in-plane total energies were more than two orders of magnitude lower than E_{MA}, in agreement with the uniaxial character of anisotropy in M-type hexaferrites.

In practice, E_{MA} consists of two parts: a contribution arising due to the presence of spin-orbit coupling and a contribution resulting from the interaction of an atomic moment with the dipolar magnetic field of atoms in the whole crystal. The first contribution was calculated using a second-variational method (as implemented in WIEN2K), which included the spin-orbit interaction within the atomic spheres. In calculations of unit cells with periodic boundary conditions, the evaluation of the latter (dipole-dipole) contribution reduced to the summation of atomic contributions within a Lorentz sphere—in our case, the value of this dipolar contribution was well converged for a sphere with a radius of 256 atomic units. The total magnetic anisotropy energies as sums of both contributions in units of meV/unit cell are displayed in the bottom row of Table V. In all studied cases, the dipolar anisotropies were of the order of 1–10 μeV/unit cell, i.e., two or more orders of magnitude smaller than the contribution due to spin-orbit interactions.

The calculated energy of the magnetocrystalline anisotropy of the Sr hexaferrite, $E_{MA} = 0.78$ meV/unit cell (Table V), corresponds to an anisotropy constant $K_1 = 0.18$ MJ/m^3 (roughly half of the experimental value 0.33 MJ/m^3, Refs. [37,38]) and is in a good agreement with the value 0.84 meV/unit cell calculated by Liyanage *et al.* using DFT with PAW potentials [15]. The anisotropy calculated for the localized solution of La hexaferrite is two times higher than that of the Sr hexaferrite, while the delocalized solution of the La hexaferrite has an anisotropy two times weaker than SrM. The localized solution of the La hexaferrite has thus more than four times higher calculated anisotropy than the delocalized

TABLE V. The contributions of individual iron sublattices to the magnetocrystalline anisotropy energy E_{MA} were calculated for the studied La and Sr hexaferrites. Due to the reduced symmetry when the magnetization is along [100], the 12k sites split with ratio 4:8 into two species $12k_1$ and $12k_2$.

	E_{MA} of sublattice (meV/cell)			E_{MA} per atom (meV)		
atom	SrM	LaM loc.	LaM deloc.	SrM	LaM loc.	LaM deloc.
Fe(2a)	−0.01	1.11	0.66	−0.01	0.56	0.33
Fe(2b)	0.48	0.24	0.42	0.24	0.12	0.21
Fe($4f_{IV}$)	0.04	−0.02	0.00	0.01	0.00	0.00
Fe($4f_{VI}$)	−0.02	0.02	0.00	−0.01	0.01	0.00
Fe($12k_1$)	0.09	0.17	0.03	0.02	0.04	0.01
Fe($12k_2$)	0.20	0.03	−0.75	0.02	0.00	−0.09
total	0.78	1.55	0.37			

solution. This result can be confronted with the experimental estimation of magnetocrystalline anisotropy by Grössinger *et al.* [20] who measured the temperature dependence of the anisotropy field of La and Sr hexaferrite powders. While for the Sr hexaferrite the authors found an anisotropy field of around 2 T which is almost constant up to 500 K, the La hexaferrite displayed a relatively monotonous decrease of the field from ∼4 T at low temperatures to ∼1.2 T at 500 K. Similar results were obtained already by Lotgering [19] for Ba and La hexaferrites. Despite the fact that our calculations correspond to temperature 0 K and a proper description would go beyond DFT, we draw a simple picture of the localization process with temperature. At low temperatures, the scenario corresponding to the localized Fe^{2+}(2a) solution calculated as the ground state is realized with a well established arrangement of Fe2+(2a) ions—in accordance with the observation of no dynamics of the extra valence electron by our NMR experiments. With increasing temperature, the state corresponding to the delocalized solution appears and dominates at high temperatures, which in effect substantially reduces the anisotropy of the La hexaferrite. In the Sr hexaferrite, there is no such transition and the anisotropy remains relatively temperature independent.

The calculated magnetocrystalline anisotropies can be analyzed further by a decomposition into contributions of individual Fe sublattices—since the spin-orbit interaction is enabled only within an atomic sphere, the decomposition can be achieved by including the spin-orbit interaction selectively on sets of atoms. We adopt an approach where the anisotropy energy due to the presence of spin-orbit coupling consists of "on site" (single ion), which is determined by the interaction of the orbital moment with the surrounding crystal field and is usually a dominant term, and "off site" contributions, which comprise the pairwise (e.g., pseudodipolar) interactions of orbital moments of neighboring atoms. We can thus evaluate the contribution of a given Fe sublattice from energies calculated with spin-orbit enabled on all atoms, including the particular Fe, and on all but the particular Fe atom (for details see Appendix).

The calculated contributions of Fe sublattices to E_{MA} are displayed in Table V. In the Sr hexaferrite, the largest contribution arises from the single-ion contribution of Fe(2b). The anisotropic character of 2b bipyramidal site is expected from the geometry of the oxygen hexahedron—strong elongation along its local axis (parallel to hexagonal axis of the unit cell) imposes large single-ion contribution to the uniaxial anisotropy. When considering E_{MA} per atom, the anisotropies of other Fe sublattices in SrM are almost an order of magnitude weaker than the anisotropy of Fe(2b), however, their total contribution is not negligible due to the larger number of atoms in the respective sublattices, especially in the case of Fe(12k). These outcomes are in accord with the generally accepted notion that the anisotropy in Sr and Ba hexaferrites is mainly due to the Fe(2b) contributions but also due to contributions of other Fe ions [8–10], although our results differ in the sign of 12k anisotropy from those obtained by means of a point charge model for the crystal field [9].

Despite the substitution of La for Sr in close vicinity to 2b sites, the contribution of Fe(2b) to the anisotropy remains large also for both La solutions. A considerable increase of anisotropy is, however, observed in the La hexaferrite due to the contribution of localized Fe^{2+}(2a) ions, whose calculated single-ion anisotropy is 1.19 meV (the contribution from the pair term is −0.08 meV).

In the delocalized solution for LaM, the extra valence charge is distributed among several sites, mainly Fe(2a) and Fe(12k), as is evidenced by the reduced (formal) valences compared to SrM (in Table III). As a consequence, the Fe(2a) and Fe(12k) contributions to anisotropy are substantially reduced. The single-ion contribution of Fe(2a) reduces to 0.87 meV (the pair-interaction term is −0.21 meV) and for Fe(12k) the single-ion term even becomes negative, −0.68 meV (the pair-interaction term is −0.07 meV).

The following text qualitatively explains the values of Fe^{2+}(2a) and Fe(12k) contributions from considerations of the site symmetry and charge density plots. In case of Fe^{2+}(2a), the single-ion contribution to anisotropy can be understood within the crystal-field theory [39]. The orbital moments of Fe are largely quenched and the orientation of 3*d* orbitals is governed by the crystal field, to which the spin-orbit interaction is only a small correction in iron oxides. For the 2a site, the 3*d* energy levels of Fe^{2+} are split by the octahedral crystal field into lower a lying triplet and a doublet. The triplet is further split by the trigonal component of the crystal field to a singlet and a doublet—their position in energy depends on the character of the trigonal distortion. The decomposition of charge within the atomic sphere of Fe(2a) reveals that in our case it is the singlet: the extra electron is contained predominately within the d_{z^2} orbital. This can be depicted by plotting the difference of charge density between the localized and the delocalized solutions [Fig. 5(b)]. Contrary to the typical setting of local axes in octahedron, here, the axes do not point toward the oxygen ligands: the distorted octahedron of the 2a site possesses trigonal symmetry with the *z* axis parallel to the global hexagonal axis of the crystal. The ground state of Fe^{2+}(2a) is the d_{z^2} singlet and its orbital moment (as well as orbital moments of other Fe) remains nearly quenched by the crystal field—all the calculated Fe orbital moments are of the order of 0.01 μ_B. For the orbital singlet d_{z^2}, even a weak spin-orbit coupling will act against the deviation of the atomic moment of the 2a iron from the trigonal axis induced by the crystal field, and as a consequence, the ion significantly increases its single-ion contribution to the anisotropy [39].

For the delocalized solution of LaM, however, the excess minority charge is smeared over various sites—notably the occupation of Fe(2a) minority band is reduced while the occupation of Fe(12k) minority band increases. This in turn decreases the large anisotropy contribution of Fe(2a) and also strongly affects the anisotropy of Fe in the 12k sites. Compared to 2a, the octahedron of the 12k site has low symmetry and an analysis analogous to the 2a case would be complicated. We thus refer only to the density plots in Fig. 5. The partial electronic charge at the 12k sites forms irregular and quite generally oriented clouds [see dark blue structures in Fig. 5(c)] with one dimension noticeably shorter than the other two. When the magnetization is set in the [100] direction, the 12k sites split into two groups 4:8. For the first group of four sites, $12k_1$, the charge clouds are favorably oriented with respect to both considered directions of magnetization [100] and [001], thus the single-ion contribution to anisotropy is almost zero. While for the eight $12k_2$ sites the clouds are slightly

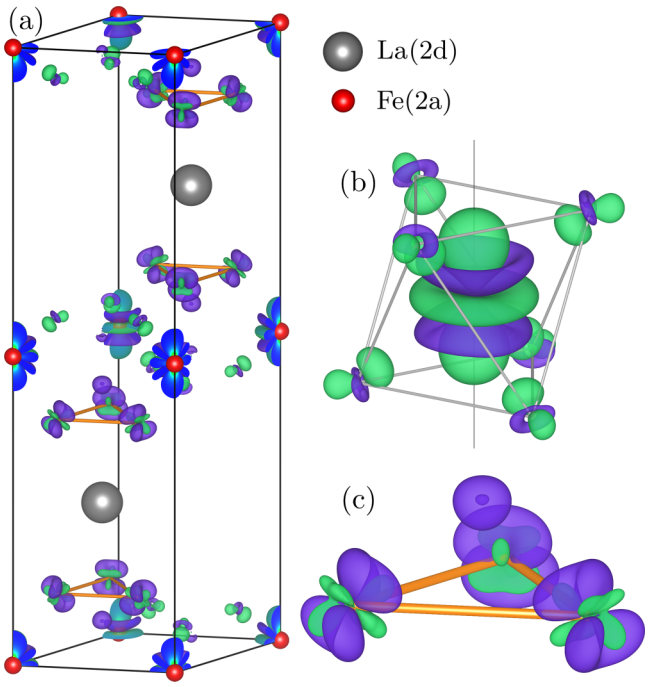

FIG. 5. (Color online) The area of the greatest difference between the localized and the delocalized solution of La hexaferrite. To construct the isosurface plot, the charge density of the delocalized solution was subtracted from that of the localized solution. Light green corresponds to areas where the charge density of the localized state is higher than the density of the delocalized state, while dark blue color corresponds to areas where the density of the delocalized state prevails. The isosurface level is 0.004 a_0^{-3} (a_0 is Bohr radius). (a) View of the hexagonal unit cell in perspective corresponding to Fig. 1. (b) The detail of the 2a site with a neighboring oxygen octahedron and (c) the detail of three of the 12k sites with one neighboring oxygen. These sites are the only sites in the unit cell where any significant difference between localized and delocalized solutions is visible.

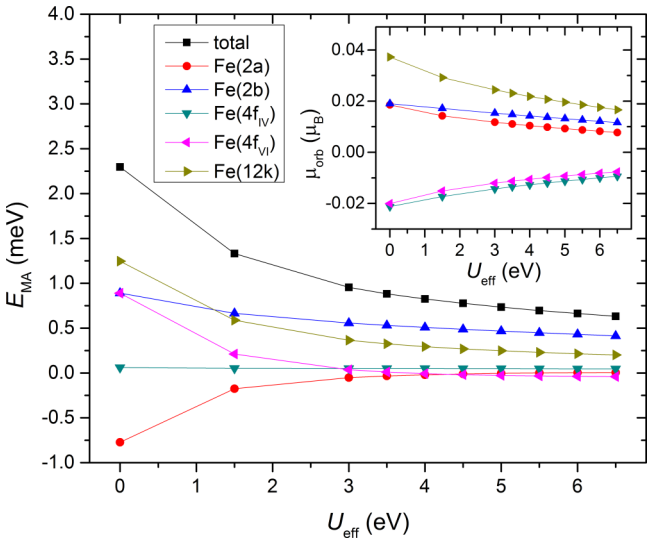

FIG. 6. (Color online) Dependence of calculated E_{MA} of Sr hexaferrite on applied U_{eff}. The inset displays an analogous dependence for the calculated orbital moments.

more prolate towards the [100] direction, which implies a negative contribution to E_{MA}. The total contribution due to the minority charge on the 12k is thus negative, which is responsible (together with decrease of positive 2a contribution) for the reduction of overall anisotropy in the delocalized La hexaferrite.

We make a note concerning the accuracy of the presented anisotropy results with respect to the used k mesh and U_{eff}. Quite surprisingly, a relatively small number of k points was needed for sufficient convergence of the calculated anisotropy, however, the k mesh used in this work ($7 \times 7 \times 1$) is consistent with other calculations of anisotropy in Sr hexaferrites [15,40]. Liyange *et al.* [15] used a $7 \times 7 \times 1$ mesh for the calculation of anisotropy in Zn- and Sb-doped Sr hexaferrites, and Feng *et al.* [40] used an $8 \times 8 \times 1$ mesh for the case of Ti- and Co-doped Sr hexaferrite. This is due to the fact that the studied hexaferrites are relatively insulating (calculated gap ~2 eV) and the occupied Fe 3*d* states are quite localized.

Also, we point out that our calculated anisotropy is sensitive to the value of U_{eff}. With increasing U_{eff}, the occupied 3*d* states become more localized and the orbital moments are reduced, which in turn reduces the anisotropy. Varying the value of U_{eff} in the range 3–6 eV, which are reasonable values for iron oxides, induces monotonous changes to the orbital moments and anisotropies by ≈20% (see Fig. 6). The trend scales in the same way for all Fe ions, therefore, we believe this dependence on U_{eff} does not impair our conclusions, at least in a qualitative level.

IV. CONCLUSIONS

The ground state with Fe^{2+} localized in 2a sites and an excited state with the charge delocalized were realized in calculations of the electronic structure of La, Nd, and Pr hexaferrites, and the localized state was observed in the spectra of ^{57}Fe nuclear magnetic resonance at 4.2 K. The preference of the extra valence charge for 2a sites was found independent on the type of the trivalent cation A^{3+} (A = La, Nd, and Pr). Apparently, the fraction of Fe^{3+}(2a) ions increases with increasing concentration of A^{3+} in the Sr hexaferrite, and at low temperatures the arrangement of ferric and ferrous ions within the 2a sublattice is static.

The magnetocrystalline anisotropy of Sr and La hexaferrites was calculated within the force theorem approach. For La hexaferrite with localized Fe^{2+}(2a), the calculated anisotropy is twice the value of the Sr hexaferrite, while the La hexaferite with delocalized electrons has half the value of the Sr hexaferrite, which is in agreement with the temperature dependence of anisotropy fields obtained in experiment [20]. From calculations of the individual Fe sites contributions to the anisotropy, we conclude that the increased anisotropy of the La hexaferrite at low temperatures is due to the single-ion contribution of 2a sites; the contributions of Fe in 2b remain appreciable in all cases. The Fe ions in 2a and 12k sites are the most affected by delocalization and are thus responsible for the decrease of anisotropy in La hexaferrites with increasing temperature.

ACKNOWLEDGMENTS

We thank to Pavel Novák from Institute of Physics ASCR for valuable discussions regarding the calculations of magnetocrystalline anisotropy. Support by the project P204-12-P352 of the Grant Agency of the Czech Republic is acknowledged. Computational resources were provided by the MetaCentrum under the program LM2010005 and the CERIT-SC under the program Centre CERIT Scientific Cloud, part of the Operational Program Research and Development for Innovations, Reg. No. CZ.1.05/3.2.00/08.0144.

APPENDIX: CALCULATION OF ATOMIC CONTRIBUTIONS TO MAGNETOCRYSTALLINE ANISOTROPY

The energy relevant for the anisotropy due to the presence of spin-orbit coupling can be expressed as (**n** is the direction of magnetization)

$$E(\mathbf{n}) = E^{\mathrm{ion}}(\mathbf{n}) + E^{\mathrm{pair}}(\mathbf{n}), \tag{A1}$$

where $E^{\mathrm{ion}}(\mathbf{n})$ represents the "on-site" contribution to anisotropy (single-ion contribution), and $E^{\mathrm{pair}}(\mathbf{n})$ denotes all "off-site" contributions appearing due to spin-orbit interaction (all pair interactions that may contribute to anisotropy, e.g., pseudodipolar interaction).

The single-ion contribution is a simple sum of all N individual atomic contributions e_i,

$$E^{\mathrm{ion}}(\mathbf{n}) = \sum_{i=1}^{N} E_i^{\mathrm{ion}}(\mathbf{n}), \tag{A2}$$

while the pair interactions take the form

$$E^{\mathrm{pair}}(\mathbf{n}) = \frac{1}{2}\sum_{i\neq j}^{N} P_{ij}\mu_i(\mathbf{n})\mu_j(\mathbf{n}), \tag{A3}$$

where P is a tensor describing these pair interactions and μ_i and μ_j are the magnetic moments of ith and jth atoms. The spin component of μ_i and μ_j is virtually unaffected by enabling of the spin-orbit interaction non-self-consistently, while the orbital momentum at a given atom emerges in the calculations only when the spin-orbit interaction is enabled for the atom. As a consequence, the vast majority of $E^{\mathrm{pair}}(\mathbf{n})$ is in fact isotropic and the anisotropy is due to orbital moments emerging when the spin-orbit interaction is present at a given atom. Therefore in calculations, when the spin-orbit is disabled for a particular atom, such an atom does not contribute to anisotropy through the pair interactions. Here, by "atom" we mean one particular sort of equivalent atoms; any contribution from pair interactions within such a sort of atoms cannot be further distinguished from the on-site ("single-ion") contribution to anisotropy. (However, such a contribution cancels out if the pair of equivalent atoms possesses a center of inversion.)

The magnetocrystalline anisotropy energy (due to spin-orbit interaction) for the whole hexaferrite cell is thus the difference of $E(\mathbf{n})$ for **n** along and perpendicular to the hexagonal axis:

$$\begin{aligned} E_{\mathrm{MA}} = E^{\perp} - E^{\parallel} &= \sum_{i}^{N}\left(E_i^{\mathrm{ion},\perp} - E_i^{\mathrm{ion},\parallel}\right) \\ &+ \frac{1}{2}\sum_{i\neq j}^{N}\left(P_{ij}\mu_i^{\perp}\mu_j^{\perp} - P_{ij}\mu_i^{\parallel}\mu_j^{\parallel}\right) = E_{\mathrm{MA}}^{\mathrm{ion}} + E_{\mathrm{MA}}^{\mathrm{pair}}. \end{aligned} \tag{A4}$$

Such quantity is calculated when the spin-orbit interaction is enabled for all atoms. In order to evaluate the individual contributions, one has to disable the spin-orbit interaction on some of the atoms and compare the results.

When the spin-orbit interaction is enabled only for kth atomic sphere and disabled for the rest, we obtain the energy

$$E_{\mathrm{MA},k}^{(1)} = \left(E_k^{\mathrm{ion},\perp} - E_k^{\mathrm{ion},\parallel}\right) = E_{\mathrm{MA},k}^{\mathrm{ion}}; \tag{A5}$$

the pair-interaction term vanishes, since only the kth orbital moment is nonzero; thus we calculate only the single-ion contribution.

To obtain the pair-interaction contribution, the setting can be inverted, i.e., we can calculate the energy for the situation with spin-orbit interaction disabled for the kth atomic sphere and enabled for the rest. Then, we get the contribution of kth atom by subtracting this energy from the energy E_{MA} where the spin-orbit interaction was enabled for all atoms:

$$\begin{aligned} E_{\mathrm{MA},k}^{(2)} &= E_{\mathrm{MA}} - \left(\sum_{i\neq k}^{N}\left(E_i^{\mathrm{ion},\perp} - E_i^{\mathrm{ion},\parallel}\right)\right. \\ &\left. + \frac{1}{2}\sum_{i\neq j;i,j\neq k}^{N}\left(P_{ij}\mu_i^{\perp}\mu_j^{\perp} - P_{ij}\mu_i^{\parallel}\mu_j^{\parallel}\right)\right) \\ &= E_k^{\mathrm{ion},\perp} - E_k^{\mathrm{ion},\parallel} + \frac{1}{2}\sum_{i\neq k}^{N}\left(P_{ik}\mu_i^{\perp}\mu_k^{\perp} - P_{ik}\mu_i^{\parallel}\mu_k^{\parallel}\right) \\ &+ \frac{1}{2}\sum_{j\neq k}^{N}\left(P_{kj}\mu_k^{\perp}\mu_j^{\perp} - P_{kj}\mu_k^{\parallel}\mu_j^{\parallel}\right) \\ &= E_{\mathrm{MA},k}^{\mathrm{ion}} + 2E_{\mathrm{MA},k}^{\mathrm{pair}}. \end{aligned} \tag{A6}$$

While the $E_k^{(1)}$ was lacking the pair-interaction contribution, $E_k^{(2)}$ contains it twice.

The pair-interaction contribution to anisotropy can now be expressed as

$$\tfrac{1}{2}\left(E_k^{(2)} - E_k^{(1)}\right). \tag{A7}$$

Eventually, the contribution of kth atom to the magnetocrystalline anisotropy (arising due to spin-orbit interaction) is calculated as

$$E_k = \tfrac{1}{2}\left(E_k^{(1)} + E_k^{(2)}\right). \tag{A8}$$

[1] H. Kojima, *Ferromagnetic Materials. A Handbook of the Properties of Magnetically Ordered Substances*, edited by E. P. Wohlfarth (North Holland, Amsterdam, 1982), Vol. 3, Chap. 5.

[2] M. Sugimoto, *Ferromagnetic Materials. A Handbook of the Properties of Magnetically Ordered Substances*, edited by E. P. Wohlfarth (North Holland, Amsterdam, 1982), Vol. 3, Chap. 6.

[3] E. Pollert, Prog. Cryst. Growth Charact. Mater. **11**, 155 (1985).

[4] R. C. Pullar, Prog. Mater. Sci. **57**, 1191 (2012).

[5] D. H. Han, Z. Yang, H. X. Zeng, X. Z. Zhou, and A. H. Morrish, J. Magn. Magn. Mater. **137**, 191 (1994).

[6] X. Batlle, X. Obradors, J. Rodríguez-Carvajal, M. Pernet, M. V. Cabañas, and M. Vallet, J. Appl. Phys. **70**, 1614 (1991).

[7] Z. W. Li, C. K. Ong, Z. Yang, F. L. Wei, X. Z. Zhou, J. H. Zhao, and A. H. Morrish, Phys. Rev. B **62**, 6530 (2000).

[8] G. Asti and S. Rinaldi, AIP Conf. Proc. **34**, 214 (1976).

[9] Y. Xu, G.-L. Yang, D.-P. Chu, and H.-R. Zhai, Phys. Status Solidi B **157**, 685 (1990).

[10] P. Novák, Czech. J. Phys. **44**, 603 (1994).

[11] M. I. Darby and E. D. Isaac, IEEE Trans. Magn. **10**, 259 (1974).

[12] D. J. D. Bitetto, J. Appl. Phys. **35**, 3482 (1964).

[13] J. Kreisel, H. Vincent, F. Tasset, M. Paté, and J. P. Ganne, J. Magn. Magn. Mater. **224**, 17 (2001).

[14] Q. Fang, H. Bao, D. Fang, and J. Wang, J. Appl. Phys. **95**, 6360 (2004).

[15] L. S. I. Liyanage, S. Kim, Y.-K. Hong, J.-H. Park, S. C. Erwin, and S.-G. Kim, J. Magn. Magn. Mater. **348**, 75 (2013).

[16] D. Seifert, J. Töpfer, F. Langenhorst, J.-M. Le Breton, H. Chiron, and L. Lechevallier, J. Magn. Magn. Mater. **321**, 4045 (2009).

[17] J. Wang, C. Ponton, and I. Harris, J. Magn. Magn. Mater. **234**, 233 (2001).

[18] J. Wang, C. Ponton, and I. Harris, J. Alloys Compd. **403**, 104 (2005).

[19] F. K. Lotgering, J. Phys. Chem. Solids **35**, 1633 (1974).

[20] R. Grössinger, M. Küpferling, M. Haas, H. Müller, G. Wiesinger, and C. Ritter, J. Magn. Magn. Mater. **310**, 2587 (2007).

[21] C. Sauer, U. Köbler, W. Zinn, and H. Stäblein, J. Phys. Chem. Solids **39**, 1197 (1978).

[22] H. Štěpánková, J. Englich, P. Novák, and H. Lütgemeier, J. Magn. Magn. Mater. **104–107**, 409 (1992).

[23] R. Grössinger, C. T. Blanco, M. Küpferling, H. Müller, and G. Wiesinger, Physica B **327**, 202 (2003).

[24] M. Küpferling, R. Grössinger, M. W. Pieper, G. Wiesinger, H. Michor, C. Ritter, and F. Kubel, Phys. Rev. B **73**, 144408 (2006).

[25] P. Novák, K. Knížek, M. Küpferling, R. Grössinger, and M. W. Pieper, Eur. Phys. J. **43**, 509 (2005).

[26] M. Küpferling, P. Novák, K. Knížek, M. W. Pieper, R. Grossinger, G. Wiesinger, and M. Reissner, J. Appl. Phys. **97**, 10F309 (2005).

[27] P. Blaha, K. Schwarz, G. K. H. Madsen, D. Kvasnicka, and J. Luitz, *WIEN2k, An Augmented Plane Wave + Local Orbitals Program for Calculating Crystal Properties* (Techn. Universität Wien, Vienna, 2001).

[28] J. P. Perdew, K. Burke, and M. Ernzerhof, Phys. Rev. Lett. **77**, 3865 (1996).

[29] A. I. Liechtenstein, V. I. Anisimov, and J. Zaanen, Phys. Rev. B **52**, R5467 (1995).

[30] S. Abdelouahed and M. Alouani, Phys. Rev. B **79**, 054406 (2009).

[31] D. Seifert, J. Töpfer, M. Stadelbauer, R. Grössinger, and J.-M. Le Breton, J. Am. Ceram. Soc. **94**, 2109 (2011).

[32] P. Novák and J. Rusz, Phys. Rev. B **71**, 184433 (2005).

[33] C. M. Fang, F. Kools, R. Metselaar, G. de With, and R. A. de Groot, J. Phys.: Condens. Mat. **15**, 6229 (2003).

[34] M. Feng, B. Shao, Y. Lu, and X. Zuo, J. Appl. Phys. **115**, 17D908 (2014).

[35] P. Novák, I. Chaplygin, G. Seifert, S. Gemming, and R. Laskowski, Comput. Mater. Sci. **44**, 79 (2008).

[36] R. F. W. Bader, *Atoms in Molecules. A Quantum Theory* (Oxford University Press, Oxford, 1990).

[37] L. Jahn and H. G. Muller, Phys. Status Solidi **35**, 723 (1969).

[38] B. T. Shirk and W. R. Buessem, J. Appl. Phys. **40**, 1294 (1969).

[39] J. C. Slonczewski, J. Appl. Phys. **32**, S253 (1961).

[40] M. Feng, B. Shao, J. Wu, and X. Zuo, J. Appl. Phys. **113**, 17D909 (2013).